transport may affect the observed hemispheric growth rates. A statistically significant divergence of the northern and southern hemispheric growth rates occurred during the period of the El Niño-Southern Oscillation (ENSO) event of 1986–87. This ENSO had a much stronger correlation with the growth rates of both CFCs than did the event of 1982–83. ENSO events, occurring every 4–7 years[27], are known to affect the interhemispheric transport of trace gases and have been correlated with lower than average mixing ratios of CH_3CCl_3 at Samoa[28]. Suppression of the westerly winds at 200 millibar (mb) in the upper troposphere which occurs during ENSOs[27] reduces the interhemispheric transport[29]. The variations observed in the hemispheric growth rates for both CFCs correlate well with hemispheric variations recently noted for methane[30] during 1986–89. A reason that the ENSO of 1986–87 had such a strong effect on the growth rates may be the coincidences of a quasi-biennial oscillation event (QBO), typically occurring every 26 months[29], followed by the strongest cold event in 15 years, the La Niña[27] of 1988–89. Also, there is a good correlation between the maximum of easterly winds of the equatorial stratosphere[31] (QBOs) and the drop in the southern hemispheric growth rate for both CFCs (Fig. 3). Although there is considerable evidence of tropospheric QBOs[32], dynamic models also show that strong easterly winds in the stratosphere can enhance vertical transport upward from the troposphere[33] and concurrently decrease the north to south tropospheric exchange[29]. As the mixing ratios of the CFCs have always been higher in the northern than southern hemisphere, any process that inhibits interhemispheric exchange or enhances tropospheric–stratosphere exchange will slow the growth rates in the southern hemisphere.

These decreased overall growth rates are encouraging in light of voluntary national and international efforts to limit emissions of ozone-depleting substances. Note that a recent report[14] also observed decreased atmospheric growth rates for the two dominant atmospheric halons, which are used primarily in fire extinguishers, and pose a significant threat to stratospheric ozone, although less than that posed by the CFCs considered here. Furthermore, continuous monitoring of CFCs, together with accurate tracking of emissions, will help to define the chemical lifetimes of these species and may provide a more complete understanding of the transport properties of the atmosphere. □

Received 30 June 1992; accepted 7 July 1993.

1. Farman, J. C., Gardiner, B. G. & Shanklin, J. D. *Nature* **315,** 207–210 (1985).
2. Molina, M. J. & Rowland, F. S. *Nature* **249,** 810–814 (1974).
3. *Montreal Protocol to Reduce Substances that Deplete the Ozone Layer Report, Final Report* (UN Environmental Programme, New York, 1987).
4. Gamlen, P. H., Lane, B. C., Midgley, P. M. & Steed, J. M. *Atmos. Envir.* **20(6),** 1077–1085 (1986).
5. Prather, M. J. & Watson, R. T. *Nature* **344,** 729–734 (1990).
6. McFarland, M. & Kaye, J. A. rev. *J. Photochem. Photobiol.* **55,** 911–929 (1992).
7. *Chlorofluorocarbons (CFC's) 11 and 12* (Alternative Fluorocarbons Envir. Acceptability Study, Washington DC, 1991).
8. Thompson, T. M., Komhyr, W. D. & Dutton, E. G. *Chlorofluorocarbon-11,-12, and Nitrous Oxide Measurements at the NOAA/GMCC Baseline Stations (16 Sept. 1973 to 31 Dec. 1979) NOAA Tech. Rep. ERL 428-ARL 8* (NOAA Air Resources Lab., Boulder, 1985).
9. Elkins, J. W. & Rossen, R. (eds) *Summary Report 1988: Geophysical Monitoring for Climatic Change* Vol. 17 (NOAA Air Resources Lab., Boulder, 1989).
10. Montzka, S. M. *et al. Summary Report 1991: Climate Monitoring and Diagnostic Laboratory* Vol. 20 (eds Ferguson, E. E. & Rossen, R.) (NOAA Climate Monitoring and Diagnostic Lab., Boulder, 1992).
11. Barrie, L. A. & Hoff, R. M. *Atmos. Envir.* **18,** 2711–2722 (1984).
12. Halter, B. C., Harris, J. M. & Conway, T. J. *J. geophys. Res.* **93(D12),** 15914–15918 (1988).
13. *Concentrations, Lifetimes, and Trends of CFCs, Halons, and Related Molecules in the Atmosphere, NASA Tech. Rep.* (in the press) (NASA, Washington DC, 1993).
14. Butler, J. H., Elkins, J. W., Hall, B. D., Cummings, S. O. & Montzka, S. A. *Nature* **359,** 403–405 (1992).
15. Goldan, P. D., Kuster, W. C. Albritton, D. L. & Schmeltekopf, A. L. *J. geophys. Res.* **85(C1),** 413–423 (1980).
16. Fabian, P., Borcher, R., Penkett, S. A. & Prosser N. J. D. *Nature* **294,** 733–735 (1981).
17. Fabian, P. *et al. J. geophys. Res.* **86(C6),** 5179–5184 (1981).
18. Schmidt, U. *et al. Geophys. Res. Lett.* **18(4),** 767–770 (1991).
19. Zander, R. *et al. J. atmos. Chem.* **15,** 171–186 (1992).
20. Jacob, D. J., Prather, M. J., Wofsy, S. C. & McElroy, M. B. *J. geophys. Res.* **92(D2),** 6614–6624 (1987).
21. Cleveland, W. S. *J. Amer. Stat. Assoc.* **74,** 829–836 (1979).
22. Filliben, J. J. *Comput. Graph.* **15(3),** 199–213 (1981).
23. Efron, B. & Tibshirani R. *Science* **253,** 390–395 (1991).
24. Rasmussen, R. A. & Khalil, M. A. K. *Science* **232,** 1623–1624 (1986).
25. Cunnold, D. M. *et al. J. geophys. Res.* **91(D10),** 10797–10817 (1986).
26. Elkins, J. W., Thompson, T. M., Hall, B. D., Egan, K. B. & Butler, J. H. *Antarc. J. U. S.* **23,** 76–77 (1988).
27. Trenberth, K. E. in *Teleconnections Linking Worldwide Climate Anomalies* (eds Glantz, M., Katz, R. W. & Nicholls, N.) 13–42 (Cambridge Univ. Press, 1991).
28. Prinn, R. *et al. J. geophys. Res.* **97(D2),** 2445–2461 (1992).
29. Webster, P. J. & Holton, J. R. *J. atmos. Sci.* **39,** 722–733 (1982).
30. Steele, L. P. *et al. Nature* **358,** 313–316 (1992).
31. *Climate Diagnostics Bulletin June 1992,* Vol. 92, No. 6 (eds Koushy, V. E., Bell, G. D. & Kopman, J. D.) 7 (U.S. Dept. of Commerce/NOAA, Washington DC, 1992).
32. Trenberth, K. E. *Mon Weath. Rev.* **108,** 1370–1377 (1980).
33. Plumb, R. A. & Bell, R. C. *Q. J. R. met. Soc.* **108,** 335–352 (1982).
34. Rasmussen, R. A. & Lovelock, J. E. *J. geophys. Res.* **88(C13),** 8369–8378 (1983).
35. Novelli, P. C., Elkins, J. W. & Steele, L. P. *J. geophys. Res.* **97(D7),** 13109–13121 (1991).
36. Montzka, S. M., Myers, R. C., Butler, J. H., Elkins, J. W. & Cummings, S. O. *Geophys. Res. Lett.* **20(8),** 703–706 (1993).
37. Bullister, J. L. & Weiss, R. F. *Deep-Sea Res.* **35(5),** 839–853 (1988).

ACKNOWLEDGEMENTS. We acknowledge the contributions of all personnel involved in collecting flask samples and maintaining the EC-GC at NOAA/CMDL and cooperative stations. We also acknowledge assistance from R. A. Rasmussen, R. F. Weiss, W. D. Komhyr, E. G. Dutton, M. McFarland, P. P. Tans, P. J. Fraser, N. B. A. Trivett and S. A. Montzka. This work was supported in part by the Atmospheric Chemistry Project of NOAA's Climate and Global Change Program.

Evaluating the role of climate cooling in iceberg production and the Heinrich events

Johannes Oerlemans

Institute for Marine and Atmospheric Research, Utrecht University, Princetonplein 5, 3584 CC Utrecht, The Netherlands

BOND *et al.*[1] recently presented evidence for the frequent occurrence, in the Pleistocene epoch, of periods of massive iceberg discharge into the North Atlantic ocean ('Heinrich events'), each lasting a few thousand years. The cause of these events is uncertain, but one possibility[1] is repeated advances of the Laurentide ice sheet during episodes of cooler climate. Here I examine this idea, using a model of the Laurentide ice sheet driven by orbitally forced variations in insolation, with and without three additional 3,000-yr-long cooling episodes, imposed just before the occurrence of the three most recent Heinrich events (H1, H2 and H3). In the model, the cooling event preceding H1 (when the climate was relatively warm and deglaciation was about to begin) led to increased calving, but those preceding H2 and H3 (which occurred during the last ice age, when the climate was very cold) led to reduced iceberg calving. It thus seems unlikely that the Heinrich events generally reflect a direct response of the Laurentide ice sheet to climate cooling.

The ice sheet model I use treats the Laurentide ice sheet in a simplified geometry. It calculates the evolution of the ice sheet along four flow lines that merge in Hudson Bay. Each flowline represents a sector (Fig. 1). Topography is schematically included. This means that when cooling occurs, two ice sheets start to grow on the high ground in sector 1 (Ellesmere/Baffin Land) and sector 2 (Labrador). These sheets grow towards the coast and in the direction of Hudson Bay, and eventually start to feed into sectors 3 and 4. Free mass exchange between the sectors is achieved by setting the ice thicknesses equal at the Hudson Bay centre. Although this approach implies a poorer resolution than obtained with two-dimensional models[2,3], I believe that it is adequate for a calculation where the main interest is in ice budgets, calving rates and runoff of melt water (here melt water is understood to be surficial melt water generated on the ice sheet—not from icebergs melting in the ocean).

Ice flow is treated in a vertically integrated formulation, as has been done in many studies of glacial cycles[4–9]. There is no explicit calculation of ice temperature. Both sliding and internal deformation contribute to the ice flow. Sliding is allowed when melt water is produced at the surface. The grid-point spacing along each flowline is 50 km. The response of the bed simply

© 1993 Nature Publishing Group

FIG. 1 Four sectors of the Laurentide ice sheet, for which mass-balance and ice-flow calculations are done separately. All sectors have runoff of melt water. Calving of icebergs occurs in sectors 1 and 2 only, when the ice edge reaches deep water. The Cordilleran Ice Complex (CIC) and the Greenland Ice Sheet (GIS), which may have interacted with the Laurentide ice sheet to some extent, are not treated in the model. Outline of ice extent is for the Late Pleistocene maximum[18].

follows damped return to local isostatic equilibrium with a 5 kyr decay time.

The ice-flow model is coupled to a numerical mass-balance model[10,11]. It calculates the mass balance from an integration of the surface energy budget through an annual cycle, given climatic input including precipitation. Dependence of the energy balance on height results from a constant atmospheric temperature lapse rate and different radiative properties of atmosphere and cloud. The mass-balance model has been tested against observations from glaciers in widely differing climates[12]. The climatic input is a function of height and distance along the flow lines, and is perturbed with series of deviations of insolation, $\delta Q(t)$, and temperature, $\delta T(t)$. Single series of these quantities are assumed to characterize the entire Laurentide ice-sheet region. $\delta T(t)$ is the departure of temperature for the summer half year. It is obtained from:

$$\delta T(t) = f_{\text{green}}(a\delta Q(t) + f_{\text{ice}}A) \quad (1)$$

Here a relates the changes of temperature to the change in insolation, including all feedbacks except those associated with atmospheric greenhouse gas concentration and ice albedo. These appear separately in equation (1). The most important feedbacks assumed to be contained in a are the water-vapour feedback and seasonal snow-cover feedback. The strength of the greenhouse feedback[13,14] is denoted by f_{green}. The ice-albedo feedback (actually related to total land ice cover on the globe but in the present case assumed to be related only to the size of the Laurentide ice sheet) has strength f_{ice}. It is set proportional to a normalized measure of the land surface covered by glacier ice in North America (A) as calculated by the model.

I used values of f_{green} and a of 2 and 0.11 $\text{KW}^{-1}\,\text{m}^2$. This implies that the varying concentration of greenhouse gases during glacial cycles doubles climate sensitivity. In the calculation of the mass-balance fields, it has been assumed that precipitation at each location varies in proportion to the saturation vapour pressure of the local air temperature. This is a first-order estimate of changes in precipitation, which finds some support from ice-core analysis[15] and modelling studies[16,17].

Tuning was done by varying the strength of the albedo feedback (Fig. 2*a*). All integrations started at 125,000 years ago (zero ice volume). The best result for ice volume was obtained with $f_{\text{ice}} = 2.3$. Significantly smaller values do not produce maximum ice cover around 20,000 years ago. Larger values do not simulate the last termination (the ice sheet does not decay entirely at the beginning of the Holocene epoch). Although this model could be criticized for its simplicity in representing the Laurentide geometry, I believe that it simulates the last glacial cycle well. No strong additional destabilizing mechanisms, like extreme calving

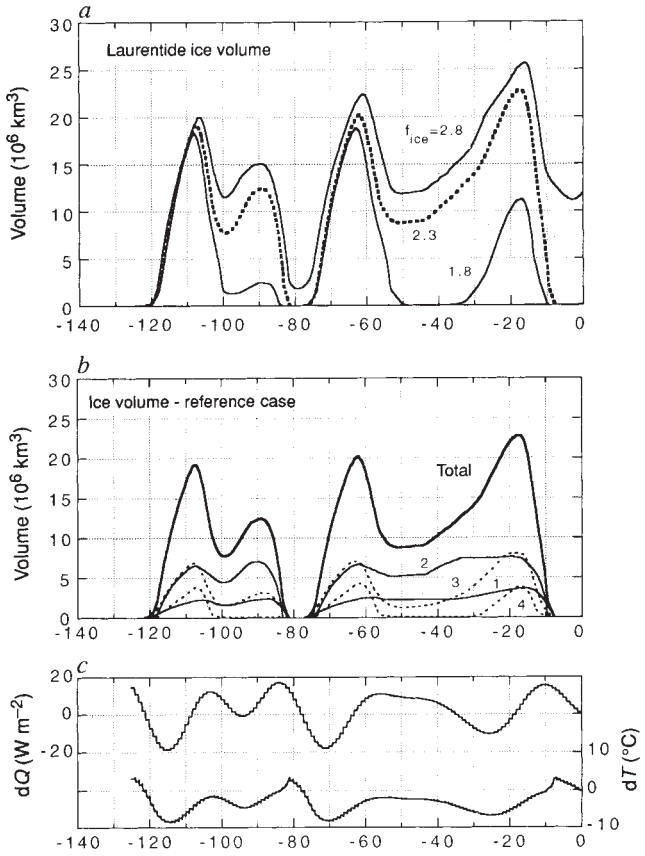

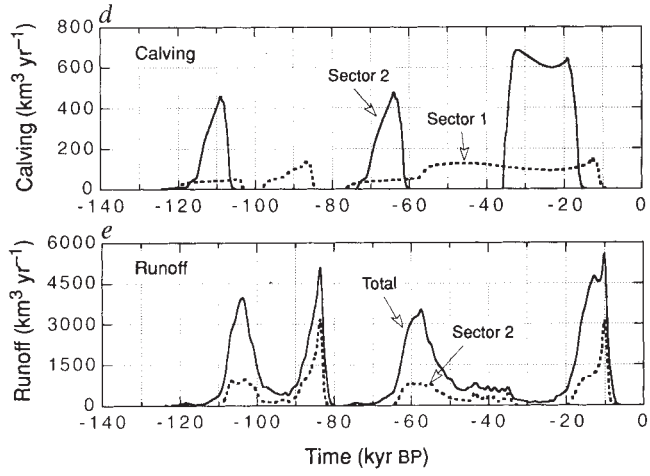

FIG. 2 *a*, The dependence of simulated Laurentide ice volume through the last glacial cycle on the ice feedback parameter f_{ice}. A value of 2.3 gives the best result, which is thus taken as the reference case. Ice volume in the four sectors for the reference case are shown in *b*. *c*, The forcing (summer insolation) and summer temperature, which depend on insolation and ice-sheet size. Calving rates and runoff of surficial melt water for the reference case are shown in *d* and *e*.

© 1993 Nature Publishing Group

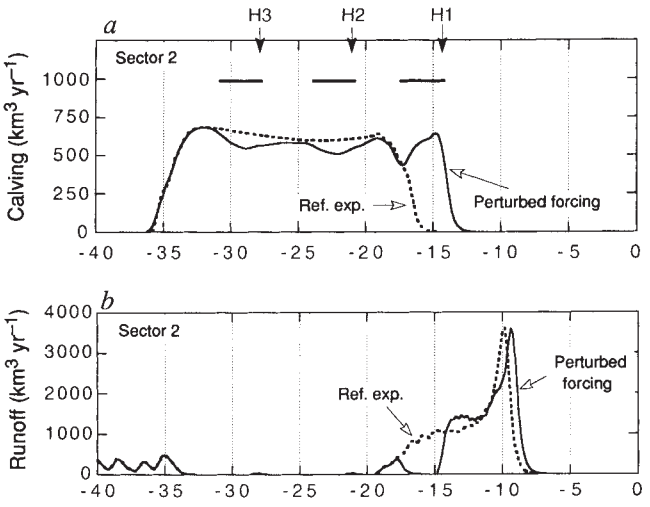

FIG. 3 Comparison of calving (*a*) and runoff (*b*) rates for the reference case and the run with imposed cooling events (labelled 'perturbed forcing'). The imposed cooling events are indicated by horizontal bars in *a*. Arrows mark the Heinrich layers[1]. The first two cooling events lead to a reduction of calving rate, the third one to a significant increase, essentially reflecting a delay of the termination.

rates or dramatic drops in ice albedo, have to be included to make the ice sheet disappear. The rapid decay rate is the result of the realistic treatment of the mass balance, leading to melt rates much higher than would be obtained by using, for instance, the equilibrium-line concept with a fixed balance gradient. Also, the inclusion of sliding when melt water is produced helps because it makes the ice-sheet somewhat flatter and lower in the ablation zone.

A further diagnosis of the run with $f_{ice} = 2.3$, referred to as the reference case, is given in Fig. 2*b*–*e*. During full glacial conditions, sectors 2 and 3 have the largest volume (Fig. 2*b*), which is a consequence of the higher snow accumulation rates as compared to sectors 1 and 4. Calculated Laurentide ice volume during the last glacial maximum is about 23×10^6 km^3. This is significantly less than values given in early reconstructions[18,19] but in agreement with later studies[20] (note that the Cordilleran ice complex is not included in the present model).

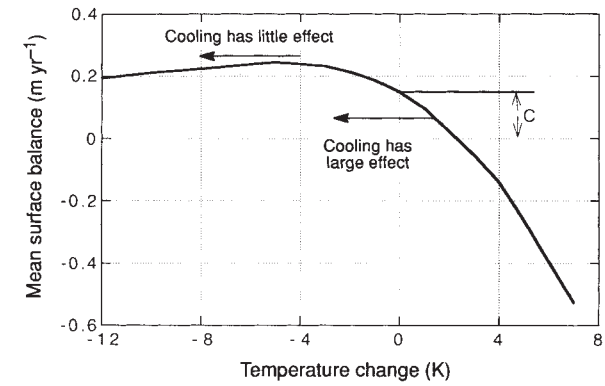

FIG. 4 The surface mass balance (*m* of water equivalent) of an ice sheet as a function of the change in atmospheric temperature. The calculation is for the Greenland ice sheet in its present state[11], but the qualitative shape of the curve is valid for any ice sheet. *C* is the equivalent amount of calving required for the ice sheet to be in balance. The effect of a cooling on the surface balance, and thus on the calving rate, depends strongly on the climatic regime present.

Orbital parameters are changed every 1,000 yr and the resulting deviation of summer radiation is shown in Fig. 2*c*, together with the departure of summer temperature. It can be seen that sharp temperature peaks occur shortly after ice-sheet decay, in agreement with the palaeoclimatic record[21,22].

Calving and runoff of melt water can be considered separately. The calving rates shown (Fig. 2*d*) are simply the flux of ice at the edge of the continent, when the ice sheet has reached this. Only sectors 1 and 2 have iceberg discharge. A typical maximum total calving rate is 700 km^3 yr^{-1}, which is in very good agreement with estimates from ice-sheet reconstruction[18]. For sector 1 the calving rate is approximately constant, whereas more pronounced variations occur in sector 2. Runoff (Fig. 2*e*) consists of melt water produced on the ice-sheet surface. It is out of phase with iceberg calving. Calving is largest when the ice sheet attains its maximum extent. When decay starts, the runoff becomes larger and larger while calving drops to zero within a few thousand years. It should be noted that typical calving rates are much smaller than typical runoff rates.

Results from the experiment with cooling events can now be compared to the reference case (Fig. 3). Anticipating on an ice-sheet response time of several kyr for this type of limited cooling, a temperature perturbation of -4 °C was imposed for 3,000 yr, starting about 3,000 yr before the ^{14}C-age of the Heinrich layers (Fig. 3*c*). I considered only the last three Heinrich layers, as these are well dated[1] (H1, 14.3 kyr BP; H2, 21 kyr BP; H3: 28 kyr BP—no correction was made to the ^{14}C-age).

The effect on ice volume (not shown) is small. Changes in calving rate for sector 2 are small and negative for H3 and H2, and large and positive for H1. The reason for lower calving rates during the first two cooling events is decreasing accumulation. As can be seen in Fig. 2*b*, the ice volume in sector 2 is fairly constant between 35,000 and 15,000 yr ago, and so is the calving rate. The imposed cooling events lead to a small perturbation only. For the cooling event starting at 11,300 yr ago the situation is totally different. The ice sheet is in a stage of rapid decay, but the cooling makes the ice sheet stay significantly longer. This then leads to a calving peak at about 15,000 yr ago.

I have run experiments with stronger and longer cooling events imposed. This requires a different tuning to keep the termination in the simulated ice-volume curve. The longer and stronger the cooling, the more the value of f_{ice} has to be reduced. Although stronger cooling events lead to larger changes in calving rates, the picture does not change in a qualitative way.

The results of this study suggest that the Heinrich layers do not result directly from the effect of cooling events on ice-sheet evolution. The effect of cooling depends on the state of the ice sheet and can have either sign. For a large ice sheet in cold conditions, additional cooling brings very little change of iceberg calving rate: it just reduces the accumulation rates slightly (H3 and H2). For a large ice sheet in warm conditions (a situation that cannot last very long), additional cooling reduces the melt rates very strongly (H1). This point is best understood by looking at a detailed mass-balance calculation for an ice sheet of given geometry (Fig. 4). When calculating the mass balance averaged over the entire ice sheet (in this case the Greenland ice sheet[11]), it becomes clear that the change of mass balance per degree temperature change becomes smaller in colder regimes (and even changes sign). □

Received 22 March; accepted 5 July 1993.

1. Bond, G. *et al. Nature* **360,** 245–249 (1992).
2. Andrews, J. T. & Mahaffy, M. A. W. *Quat. Res.* **6,** 167–183 (1976).
3. Budd, W. F. & Smith, I. N. *Sea Level, Ice, and Climatic Change* (Proc. of the Canberra Symp., Dec. 1979) IAHS Publ. No. 131, 369–409 (1981).
4. Oerlemans, J. *Nature* **287,** 430–432 (1980).
5. Pollard, D. *Nature* **296,** 334–338 (1982).
6. Oerlemans, J. *Clim. Change* **4,** 353–374 (1982).
7. Hyde, W. T. & Peltier, W. R. *J. atmos. Sci.* **44,** 1351–1374 (1985).
8. Deblonde, G. & Peltier, W. R. *J. geophys. Res.* **96,** 9189–9215 (1991).
9. Gallée, H., Van Ypersele, J. P., Fichefet, T., Tricot, C. & Berger, A. *J. geophys. Res.* **96** (D7), 13139–13161 (1991).
10. Oerlemans, J. & Hoogendoorn, N. C. *J. Glaciol.* **35,** 399–405 (1989).

© 1993 Nature Publishing Group

11. Oerlemans, J. *The Holocene* **1,** 40–49 (1991).
12. Oerlemans, J. & Fortuin, J. P. F. *Science* **258,** 115–117 (1992).
13. Broccoli, A. J. & Manabe, S. *Clim. Dynamics* **1,** 87–99 (1987).
14. Lorius, C., Jouzel, J., Raynaud, D., Hansen, J. & Le Treut, H. *Nature* **347,** 139–145 (1990).
15. Reeh, N. & Gundestrup, N. S. *J. Glaciol.* **31,** 198–200 (1985).
16. Fortuin, J. P. F. *The Surface Mass Balance and Temperature of Antarctica* (Univ. of Utrecht, The Netherlands, 1992).
17. Manabe, S. & Broccoli, A. J. *J. geophys. Res.* **90** (C2), 2167–2190 (1985).
18. Sugden, D. E. *Arctic Alp. Res.* **9,** 21–47 (1977).
19. Denton, G. H. & Hughes, D. J. *The Last Great Ice Sheets* (Wiley-Interscience, New York, 1981).
20. Fisher, D. A., Reeh, N. & Langley, K. *Geogr. phys. Quat.* **39,** 229–238 (1985).
21. Koerner, R. M. *Nature* **343,** 630–631 (1980).
22. Anderson, P. M. *et al.* (COHMAP Members) *Science* **241,** 1043–1052 (1988).

Past sedimentary organic matter accumulation and degradation controlled by productivity

Philippe Bertrand* & Elisabeth Lallier-Vergès

URA 724 CNRS, Sédimentation et Diagenèse Organique, Université d'Orléans, 45067 Orléans Cedex 2, France

CHANGES in bottom-water oxygen concentration are commonly invoked to account for past changes in sedimentary organic carbon accumulation, as organic matter is more readily preserved in anoxic conditions[1–5]. On the other hand, upper-water productivity has been shown to be the main controlling factor for accumulation of organic matter in modern sediments[6,7]. It is therefore important to understand whether productivity significantly influenced accumulation patterns in the past, for example during the formation of petroleum source rocks. Here we present a study of a 150-Myr-old sequence containing short-term cycles in organic carbon content from the Kimmeridge Clay formation in Northern England. The lack of bioturbation and the fine-scale laminations throughout this section demonstrate that the sequence was deposited under continuously anoxic bottom-water conditions, so that oxic excursions cannot account for the cyclic accumulation pattern. We show that in this cycle, increased planktonic productivity appears to have caused both increased sedimentary accumulation of refractory organic material, and increased anaerobic degradation of metobolizable organic material. Thus, upper-water productivity should be considered as an important factor in controlling past as well as present accumulation patterns.

The Kimmeridge Clay formation is well known as a lateral equivalent of the major oil source rock unit of the North Sea, outcropping in the Cleveland basin near Marton (England). It consists of alternating organic-rich shales and marls deposited in marginal shallow water under low energy conditions, and reveals a short-term cyclic distribution of the organic content[8]. These cycles (1 m thick on average) have been found to represent 30,000 years[8], which was evaluated by dividing the duration of an ammonite zone by the number of the cycles within it. One of these microcycles has been investigated by high-resolution sampling (90 samples distributed along an 120-cm-long core section). The total organic carbon content (TOC) values range between 1.8 and 9.5 weight % with the lowest values at the beginning of the cycle and the highest ones in the middle part (Fig. 1).

The TOC variations cannot be explained by a varying dilution by detrital (clay and quartz) and biogenic (mainly coccoliths, occasional diatoms) minerals[9]. Indeed, except for the biogenic carbonate content, the mineralogical and geochemical composition of the inorganic fraction of the sediment is fairly constant throughout the section, suggesting that variations of the detrital input were weak during the cycle. The carbonate content variations are not strong enough to explain TOC variations and, moreover, are not in phase with them. A diagenetic removal of minerals is also unlikely because no traces of dissolution have been observed. The sediment is fine-grained, stratified with fine-scale laminations, contains abundant sulphides, and does not exhibit any bioturbation. This last character indicates clearly that not only the sediment but also the bottom water has always been anoxic during the cycle. Indeed, in such marginal shallow waters with a high input of organic matter, the absence of heterotrophic and oxygen-dependent benthic life can be explained only by the occurrence of totally anoxic bottom waters over a significant time period. On the other hand, the fine-grained and stratified character of the sediment indicates low energy conditions which permit the development of anoxic bottom conditions when oxygen is totally consumed. The constancy of anoxic conditions are additionally indicated by inorganic markers such as the high vanadium content[9]. Molecular and petrographic investigations[10,11] have revealed that the origin of the organic matter is mainly phytoplanktonic. Therefore, as the TOC variations cannot be explained by dilution or by changes in redox conditions, they are most plausibly related to varying productivity-related organic fluxes. Moreover, the productivity variations are probably mainly due to mineral-free phytoplankton because TOC and carbonate contents (from coccoliths) variations appear to be independent.

As a consequence of bacterial sulphate reduction, reduced sulphur is often concentrated in organic-rich marine sediments. In our cyclic sequence, most of the sulphur is diagenetically trapped (both as iron sulphides and as organic sulphur compounds) and can therefore be used to estimate the fraction of organic carbon that was oxidized by sulphate reduction. In order

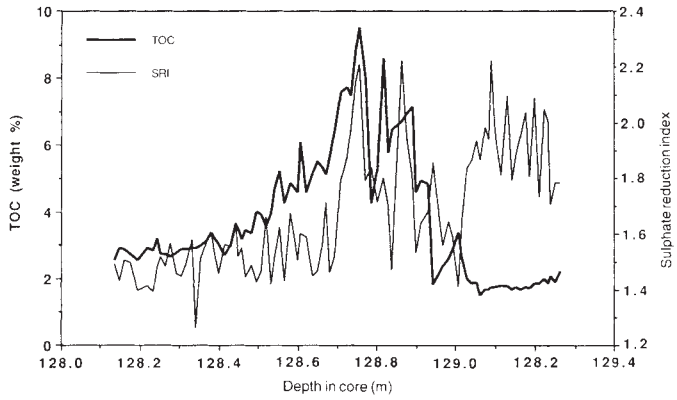

FIG. 1 Variations of total organic carbon content (TOC, in weight %) and sulphate reduction index (SRI) in the deposition cycle. SRI represents the intensity of sulphate reduction relative to the TOC. It is defined as the ratio of (organic carbon preserved + mineralized by sulphate reduction) to preserved organic carbon. Mineralized organic carbon is calculated by using the measured sulphur content and assuming the mean stoichiometry for sulphate reduction[17] $2CH_2O + SO_4^{2-} \rightarrow H_2S + 2HCO_3^-$. We can write $C_{ox} \geq 0.75$ S where C_{ox} and S denote masses of organic carbon oxidized by sulphate reduction, and reduced sulphur trapped in the sediment respectively. $C_{ox} = 0.75$ S if sulphur was trapped with perfect efficiency (100%), $C_{ox} = 7.5$ S if it was trapped with a low efficiency (10%)[17]. Some simple mathematical considerations show that the SRI, which is normally a mass or a flux ratio, can reasonably be approached by using the organic carbon and sulphur contents in the same manner. In this study, a mean of 30% of the sulphur (as H_2S produced by sulphate reduction) was assumed to be trapped in the sediment, according to $\delta^{34}S$ investigations. Comments about SRI variations are given in the text as well as the Fig. 2 legend.

* Present address: URA 197, Géologie et Océanographie, Université de Bordeaux I, 33405 Talence Cedex, France.

© 1993 Nature Publishing Group